EVALUATION OF A TECHNIQUE FOR DETERMINING AIRPLANE AILERON EFFECTIVENESS AND ROLL RATE BY USING AN AEROELASTICALLY SCALED MODEL

by Irving Abel

Langley Research Center
Langley Station, Hampton, Va.

1. Report No. NASA TN D-5538	2. Government Accession No.	3. Recipient's Catalog No.
4. Title and Subtitle EVALUATION OF A TECHNIQUE FOR DETERMINING AIRPLANE AILERON EFFECTIVENESS AND ROLL RATE BY USING AN AEROELASTICALLY SCALED MODEL		5. Report Date November 1969
		6. Performing Organization Code
7. Author(s) Irving Abel		8. Performing Organization Report No. L-6695
		10. Work Unit No. 126-14-14-09-23
9. Performing Organization Name and Address NASA Langley Research Center Hampton, Va. 23365		11. Contract or Grant No.
		13. Type of Report and Period Covered Technical Note
12. Sponsoring Agency Name and Address National Aeronautics and Space Administration Washington, D.C. 20546		
		14. Sponsoring Agency Code

15. Supplementary Notes

16. Abstract

Wind-tunnel studies of an aeroelastically and dynamically scaled model of a multijet cargo airplane have been conducted to measure aileron-control characteristics at Mach numbers up to 0.93. A successful technique has been demonstrated for determining the aileron effectiveness, reversal boundary, and flight roll rates below the reversal boundary based on measured values of damping in roll.

17. Key Words Suggested by Author(s) Aeroelastic model Aileron effectiveness Roll rate	18. Distribution Statement Unclassified — Unlimited		
19. Security Classif. (of this report) Unclassified	20. Security Classif. (of this page) Unclassified	21. No. of Pages 31	22. Price* $3.00

*For sale by the Clearinghouse for Federal Scientific and Technical Information
Springfield, Virginia 22151

EVALUATION OF A TECHNIQUE FOR DETERMINING AIRPLANE
AILERON EFFECTIVENESS AND ROLL RATE BY USING
AN AEROELASTICALLY SCALED MODEL

By Irving Abel
Langley Research Center

SUMMARY

Aileron effectiveness, damping in roll, and predicted full-scale roll rates at selected dynamic pressures below the aileron reversal boundary have been experimentally determined on an aeroelastically scaled model of a recently developed, multijet cargo airplane. The studies were conducted in the Langley transonic dynamics tunnel at Mach numbers up to 0.93.

Results of this wind-tunnel investigation, compared with full-scale flight data, have demonstrated both a successful method for determining full-scale aileron effectiveness including the reversal boundary and a new dynamic technique for predicting flight roll rates at dynamic pressures below the reversal boundary based on measured values of aileron effectiveness and damping in roll.

INTRODUCTION

Loss of aileron control on an airplane can occur due to deformation of the wing under the action of aerodynamic loads resulting from aileron deflections. When the aerodynamic forces due to wing deformation and aileron displacement combine to produce a value of zero rolling moment, the condition is referred to as aileron reversal. For dynamic pressures (constant Mach number) slightly above this point, the effect of the ailerons is reversed from the normal effect.

Theoretical prediction of the reversal boundary becomes very difficult in the transonic speed range where existing aerodynamic theories are inadequate. For example, during the early design stages of a recently developed, multijet cargo airplane, aileron-effectiveness studies were conducted on a low-speed flutter model. (See ref. 1.) These studies indicated sufficient operating margin. Analytical studies based on later aerodynamic data (also discussed in ref. 1) indicated a lower reversal boundary than the previous low-speed studies had indicated. In view of these results, transonic wind-tunnel studies of a complete aeroelastically scaled high-speed flutter model were initiated.

(See refs. 1 and 2.) It is interesting to note that Guyett in reference 3 states that flexible models of this type have not been widely used in the design stage to estimate aileron effectiveness even though control power in roll has dictated the wing stiffness on many airplanes.

The static experimental technique presented in references 1 and 2 is useful in determining the aileron effectiveness, including the reversal boundary. However, the airplane designer is also interested in knowing the roll rate produced by a static deflection of the ailerons. Since this problem is dynamic in nature, it cannot be experimentally determined from static measurements alone.

The purpose of this report is twofold: first, to evaluate by comparison with flight data the use of an aeroelastically scaled model for determining the aileron reversal boundary; and, second, to present and evaluate a new dynamic technique for establishing aileron effectiveness and roll damping at conditions below the reversal boundary so that full-scale roll rate can be experimentally predicted from an aeroelastically scaled model.

The basic wind-tunnel approach to determine the aileron effectiveness consists of measuring the static rolling moment generated by the model for a known aileron deflection. Two static experimental techniques are presented which differ in the manner that the model is mounted in the wind tunnel and the rolling moments determined. One method uses the sting-pylon-spring mount discussed by Grosser in reference 2, and the second method uses the two-cable mount system presented by Reed and Abbott in reference 4.

The dynamic technique used to determine the aileron effectiveness C_{l_δ} and damping in roll C_{l_p} utilizes the two-cable mount system. The technique is, in principle, similar to that used in flight tests, namely, measuring the response of the model to known control inputs. In this study, the dynamic response of the model to a sinusoidal deflection of the ailerons was measured. Reference 5 shows that, by properly selecting a suitable elastic-axis location for the mount system, the dynamic response of the configuration to a sinusoidal deflection of the ailerons can be approximated by a single degree of freedom at dynamic pressures somewhat below the reversal boundary. In order to verify both the static and dynamic techniques, the aileron reversal boundary and the predicted roll rates at dynamic pressures below the boundary, based on model measurements, are compared with full-scale flight data.

SYMBOLS

Measurements for this investigation were taken in the U.S. Customary System of Units. Equivalent values are indicated herein in the International System (SI). Details concerning the use of SI units, together with physical constants and conversion factors, are given in reference 6.

a   longitudinal distance between model center of gravity and outer cable-tangency point on rear pulleys, feet (meters)

b   wing span, feet (meters)

C_l rolling-moment coefficient, M_X/qSb

C_{l_p} damping-in-roll stability derivative, $\partial C_l \big/ \partial\!\left(\dfrac{\dot{\varphi}b}{2U}\right)$

C_{l_δ} aileron-effectiveness derivative, $\partial C_l/\partial\delta_a$

c   longitudinal distance between model center of gravity and outer cable-tangency point on front pulleys, feet (meters)

$\bar{c}$ length of wing mean aerodynamic chord, feet (meters)

d   longitudinal distance between model plane of symmetry and outer cable-tangency points on rear pulleys, feet (meters)

EI   bending stiffness, pound-inches^2 (kilonewton-meters^2)

e   base of natural system of logarithms, 2.71828

GJ   torsional stiffness, pound-inches^2 (kilonewton-meters^2)

g   acceleration due to gravity

h   vertical distance between model center of gravity and outer cable-tangency point on front pulleys, feet (meters)

I_X, I_Y, I_Z moment of inertia about X-, Y-, and Z-axis, respectively, slug-feet^2 (kilogram-meters^2)

$i = \sqrt{-1}$

j   index referring to a discrete frequency

$K_{\varphi\varphi}$ cable-stiffness influence coefficient in roll, foot-pounds/radian (meter-newtons/radian)

3

k	reduced frequency, $\omega\bar{c}/2U$
L_f, L_r	length of cable from wall-attachment point to outer cable-tangency point on front and rear pulley, respectively, feet (meters)
M	Mach number
M_X, M_Y, M_Z	rolling, pitching, and yawing moment, respectively
N	number of discrete frequency data points at each test condition
q	dynamic pressure, $\frac{1}{2}\rho U^2$, pounds/foot^2 (kilonewtons/meter^2)
S	wing area, square feet (meters^2)
T_f, T_r	tension in front and rear cables, respectively, pounds (newtons)
t	time, seconds
U	wind-tunnel flow velocity, feet/second (meters/second)
V_D	limit dive speed
X,Y,Z	model axis system with origin at center of gravity
z_p	displacement of rear cable-attachment point along tunnel wall, feet (meters)
$\bar{\alpha}$	phase angle between aileron displacement and roll angle, degrees
β_f	angle in vertical plane between X-axis and front cables, degrees
β_r	angle in horizontal plane between X-axis and rear cables, degrees
δ_a	aileron displacement from neutral position (positive when right aileron trailing edge is up), degrees or radians
θ_t	model trim angle
ρ	mass density of wind-tunnel test medium, slugs/foot^3 (kilograms/meter^3)

4

φ,ψ,θ roll angle, yaw angle, and pitch angle, respectively, radians

φ_O dynamic roll amplitude, radians

ω circular frequency, radians/second

$|\ |$ denotes absolute value

Subscripts:

A   airplane

M   model

Superscript:

*   complex conjugate

A single dot over a symbol denotes a first derivative with respect to time and double dots denote a second derivative with respect to time.

APPARATUS

Tunnel

The investigation was conducted in the Langley transonic dynamics tunnel which has a 16-foot-square (4.88-meter) test section (with cropped corners) and is a return-flow, variable-pressure, slotted-throat wind tunnel. It is capable of operation at stagnation pressures from near vacuum to slightly above atmospheric and at Mach numbers from 0 to 1.2. Mach number and dynamic pressure can be varied independently with either air or Freon-12 used as the test medium. All wind-tunnel test results presented in this investigation were conducted with Freon-12 used as the test medium.

Model Description

A 1/19-size, complete, aeroelastically scaled flutter model of a recently developed, multijet cargo airplane was used for this investigation. A three-view drawing of the model is presented in figure 1. A photograph of the model on the two-cable mount system is presented in figure 2. The model was geometrically, dynamically, and elastically scaled to simulate in Freon-12, a Mach number and altitude condition of the full-scale airplane in flight. The Froude number was not scaled. Geometric and mass properties

5

of the model are presented in table I. Scale factors relating the model to the full-scale airplane are presented in table II.

Model Design

The wings were of a magnesium box-spar construction representing scaled stiffness. Spar-stiffness distribution in bending and torsion, compared with design, is presented in figure 3. Proper aerodynamic contours were achieved by attaching balsa fairings to the spar. The balsa fairings are segmented spanwise to reduce any significant stiffness contribution to the scaled spar. A cutaway view of a typical spar section is presented in figure 4. The stiffnesses of the model fuselage, fin, stabilizer, and control surfaces were represented in a similar manner.

The model had trailing-edge 24-percent-chord ailerons extending from 68-percent to 100-percent wing span. The aileron-surface and actuator stiffnesses were scaled. The gap between the wing and ailerons was aerodynamically sealed. Independent roll control was provided by wing spoiler panels. The arrangement of these panels did not represent an airplane configuration. Since elevators were not simulated, pitch control was provided by an all-movable horizontal stabilizer. The ailerons, spoilers, and horizontal tail were all remotely operated. During a portion of the test program the aileron drive mechanism was modified to provide an oscillatory deflection of variable frequency and fixed amplitude.

Mount Descriptions

Two-cable mount system.- Reed and Abbott (ref. 4) describe the basic two-cable mount system. A schematic representation of the model on the mount is presented in figure 5(a). Details of the mount are given in figure 5(b). The mount system consists of two mutually perpendicular cable loops, one extending upstream and one downstream, which attach to the tunnel walls. For this investigation the front cable is in the vertical plane and the rear cable is in the horizontal plane. Each cable loop passes through pulleys attached to the fuselage spar. The cables are kept under tension by stretching a soft spring in the rear cable loop. In this configuration the model has five degrees of freedom (fore and aft motion restricted).

In order to use the two-cable mount system in this investigation, a convenient manner is required for measuring model static rolling moments generated by the ailerons. This is accomplished by moving the downstream attachment points of the rear cable in opposite directions along the tunnel walls (fig. 6). A differential deflection of the rear cable produces a restoring moment applied to the model. The rear cable is deflected by passing each leg through a separate pulley assembly which traverses on a shaft mounted to the tunnel wall. The pulley assemblies are displaced by a remotely operated drive system. Trim controls for longitudinal and lateral motions are provided on the model by a remotely operated horizontal tail and wing spoiler panels, respectively.

6

As a precaution against loss of the entire model due to either a flight instability or model failure, four small-diameter steel cables are attached to the model fuselage to provide emergency restraint. (See fig. 2.) These cables, which are normally slack, extend through the tunnel walls and can be actuated remotely to secure the model.

Sting-pylon-spring mount system.- Grosser (ref. 2) describes the sting-pylon-spring model support used during part of this investigation. As shown in figure 7, the mount consists of a tubular sting which is attached on the downstream end to the tunnel model support and pivoted on a frame near the upstream end. A pair of pylons extend from the top of the sting into the model fuselage contour. Attached to each of the pylons is a pair of leaf springs which connect, through other leaf springs, to the model fuselage spar. These springs provide the model with limited six degrees of freedom. The leaf springs provide a means for adjusting mount stiffnesses to insure rigid body stability.

Drag on the model is compensated remotely by varying tension in a thrust cable which is attached to the fuselage spar by coil springs. Roll rods extend from a strain-gaged balance mechanism within the sting and connect to the model fuselage spar through ball joints. The balance mechanism is arranged so that it imposes only a restraint in roll. Rolling moments generated by the model are transferred by the roll rods to the balance for direct measurements. As an added feature, the roll mechanism can be rotated remotely to provide roll trim. Longitudinal trim is provided by remotely varying the horizontal-tail incidence angle or by pivoting the sting. The mount is provided with mechanical stops on both pylons to limit amplitudes of motion.

Instrumentation

Instrumentation for the two-cable-mount tests included: (1) aileron-position indicators, (2) servo accelerometer oriented to measure static roll angle, (3) tension links in front and rear flying cables, (4) variable resistance potentiometer to measure differential deflection of the rear flying cable, and (5) a miniature rate gyro oriented to measure model roll rate. Signals from the rate gyro and aileron-position indicators were recorded on magnetic tape for further analysis and simultaneously displayed on a direct-writing recorder for visual monitoring. Other signals which varied more slowly with time were digitized and tabulated on a line printer.

TEST TECHNIQUES AND ANALYSIS

Static Technique for Determining Aileron Effectiveness C_{l_δ}

The aileron effectiveness and reversal boundary at transonic speeds were experimentally determined in reference 2 by using the sting-pylon-spring mount system. With this test technique, model rolling moments generated by a deflection of the ailerons can

be measured directly from the roll balance located in the sting. The reversal boundary, as a function of dynamic pressure and Mach number, is obtained by passing a curve through the points of zero rolling moment.

During a typical test, Mach number and dynamic pressure are increased while maintaining a preselected tunnel pressure. At selected intervals the ailerons are remotely deflected through a known displacement and the resulting rolling moment is measured. This procedure is repeated until reversal is encountered or the maximum desired test point is achieved. The tunnel pressure is then changed and another Mach number variation is made.

Aileron effectiveness over a range of dynamic pressures at $M = 0.675$ and $M = 0.75$ was determined by using the two-cable mount system for comparison with the previous static results. The test technique differs from that of the sting-pylon-spring mount in the manner that rolling moments are measured. At the desired test point the model is trimmed for level flight attitude by deflecting the wing spoiler panels. The ailerons are then deflected through a known angle resulting in a model roll angle. The model is returned to its trim attitude by differentially traversing the downstream attachment points of the rear flying cable. Statically, the mount restoring moment is equivalent to the moment generated by the ailerons. The equation defining the mount restoring moment supplied by the cables (see fig. 6) is approximately

$$\text{Restoring moment} = \frac{2 T_r z_p d}{L_r} \qquad \left(z_p \ll L_r\right) \qquad (1)$$

Dynamic Technique for Determining Aileron Effectiveness C_{l_δ}

and Damping in Roll C_{l_p}

In order to estimate the aileron effectiveness and damping in roll, the following single-degree-of-freedom free-flight roll equation is assumed (ref. 7):

$$I_X \ddot{\varphi} - \frac{qSb^2}{2U} C_{l_p} \dot{\varphi} = qSbC_{l_\delta}\delta_a \qquad (2)$$

For steady-state roll, $\ddot{\varphi} = 0$; therefore, equation (2) can be written as

$$\dot{\varphi} = -\frac{C_{l_\delta}}{C_{l_p}} \frac{2U\delta_a}{b} \qquad (3)$$

The experimental prediction of free-flight roll rate requires that both the aileron-effectiveness derivative C_{l_δ} and the damping-in-roll derivative C_{l_p} be measured as a function of Mach number and dynamic pressure on an aeroelastically scaled model tested in the wind tunnel.

Reference 5 presents a wind-tunnel technique to measure both the longitudinal and lateral stability and control derivatives of a flexible model flown on the two-cable mount system. The technique discussed is similar to the free-flight approach of measuring airplane response to a control surface input. Presented in reference 5 is an approximate method of predicting the lateral derivatives C_{l_δ} and C_{l_p} at dynamic pressures below the reversal boundary. These are the derivatives required to estimate the flight roll rate from equation (3).

Reference 5 shows that, by the proper selection of mount-system geometry (selection of location of mount-system elastic axis), the model response to a sinusoidal deflection of the ailerons can be approximated by a single-degree-of-freedom equation of the form

$$I_X \ddot{\varphi} - \frac{qSb^2 C_{l_p}}{2U} \dot{\varphi} + K_{\varphi\varphi}\varphi = qSbC_{l_\delta}\delta_a \tag{4}$$

where $K_{\varphi\varphi}$ is a stiffness influence coefficient associated with the mount system.

The term $K_{\varphi\varphi}$ (see ref. 4) can be written as

$$K_{\varphi\varphi} = 2hT_f\left(\frac{h}{L_f} + \sin\beta_f\right) + 2dT_r\left(\frac{d}{L_r} + \sin\beta_r\right) \tag{5}$$

The terms comprising equation (5) are shown schematically in figure 5(b). Since the geometric terms are known quantities, the term $K_{\varphi\varphi}$ is evaluated at each test condition by measuring the front and rear cable tensions T_f and T_r, respectively.

For sinusoidal motion the aileron forcing function is

$$\delta_a(t) = \delta_a e^{i\omega t}$$

and the roll response becomes

$$\varphi(t) = \varphi_0 e^{i(\omega t + \overline{\alpha})}$$

$$\dot{\varphi}(t) = i\omega\varphi_0 e^{i(\omega t + \overline{\alpha})}$$

$$\ddot{\varphi}(t) = -\omega^2\varphi_0 e^{i(\omega t + \overline{\alpha})}$$

After canceling out $e^{i\omega t}$, equation (4) can be written as

$$i\omega\frac{qSb^2}{2U}C_{l_p}\varphi_0 e^{i\overline{\alpha}} + qSbC_{l_\delta}\delta_a = \left(-I_X\omega^2 + K_{\varphi\varphi}\right)\varphi_0 e^{i\overline{\alpha}} \tag{6}$$

Equation (6) contains the unknown derivatives C_{l_p} and C_{l_δ}. It is pointed out in reference 5 that, if the dynamic roll amplitude φ_0 and the phase angle $\bar{\alpha}$ are measured as functions of aileron frequency at each test condition, a set of redundant equations is generated from equation (6) which can be solved for the derivatives C_{l_p} and C_{l_δ} by a method of least squares. If C_{l_p} and C_{l_δ} are assumed to be independent of frequency, equation (6) becomes

$$A_{j1}C_{l_p} + A_{j2}C_{l_\delta} = b_j \tag{7}$$

where

$$
\left.
\begin{aligned}
A_{j1} &= \frac{qSb^2}{2U}\left(i\omega\varphi_0 e^{i\bar{\alpha}}\right)_{\omega=\omega_j} \\[2mm]
A_{j2} &= qSb\delta_a \\[2mm]
b_j &= \left[\left(-I_X\omega^2 + K_{\varphi\varphi}\right)\varphi_0 e^{i\bar{\alpha}}\right]_{\omega=\omega_j}
\end{aligned}
\right\}
\qquad (j = 1,2,3,\ldots N)
$$

Equation (7) is solved in reference 5 by a least-squares solution for a set of linear complex equations. This solution is similar to that for a set of linear real equations except that the residual (or deviation) is defined in terms of the absolute value of a complex expression. The solution of equation (7) is expressed as

$$
\begin{bmatrix}
2\sum\limits_{j=1}^{N}\left|A_{j1}\right|^2 & \sum\limits_{j=1}^{N}\left(A_{j1}^{*}A_{j2} + A_{j1}A_{j2}^{*}\right) \\[4mm]
\sum\limits_{j=1}^{N}\left(A_{j1}^{*}A_{j2} + A_{j1}A_{j2}^{*}\right) & 2\sum\limits_{j=1}^{N}\left|A_{j2}\right|^2
\end{bmatrix}
\begin{Bmatrix} C_{l_p} \\[2mm] C_{l_\delta} \end{Bmatrix}
=
\begin{Bmatrix}
\sum\limits_{j=1}^{N}\left(A_{j1}^{*}b_j + A_{j1}b_j^{*}\right) \\[4mm]
\sum\limits_{j=1}^{N}\left(A_{j2}^{*}b_j + A_{j2}b_j^{*}\right)
\end{Bmatrix}
$$

Substituting for A_{j1}, A_{j1}^{*}, A_{j2}, A_{j2}^{*}, b_j, and b_j^{*} and simplifying gives

$$
\begin{bmatrix}
\left(\dfrac{qSb^2}{2U}\right)^2 \sum\limits_{j=1}^{N}\left(\omega\varphi_0\right)^2_{\omega=\omega_j} & -\dfrac{q^2S^2b^3\delta_a}{2U}\sum\limits_{j=1}^{N}\left(\omega\varphi_0\sin\bar{\alpha}\right)_{\omega=\omega_j} \\[4mm]
-\dfrac{q^2S^2b^3\delta_a}{2U}\sum\limits_{j=1}^{N}\left(\omega\varphi_0\sin\bar{\alpha}\right) & \left(qSb\delta_a\right)^2 N
\end{bmatrix}
\begin{Bmatrix} C_{l_p} \\[2mm] C_{l_\delta} \end{Bmatrix}
=
\begin{Bmatrix}
0 \\[4mm]
-qSb\delta_a\sum\limits_{j=1}^{N}\left[\left(I_X\omega^2 - K_{\varphi\varphi}\right)\left(\varphi_0\cos\bar{\alpha}\right)\right]_{\omega=\omega_j}
\end{Bmatrix}
\tag{8}
$$

Equation (8) is then used to determine the derivatives C_{l_p} and C_{l_δ} based on measured model response at N discrete frequencies. The free-flight roll rate is determined from the measured values of these derivatives at the properly scaled flight condition. That is,

$$\dot{\varphi}_A = -2\left(\frac{C_{l_\delta}}{C_{l_p}}\right)_M \left(\frac{U\delta_a}{b}\right)_A \tag{9}$$

where

$$U_A = \frac{U_M}{0.416}$$

$$b_A = \frac{b_M}{0.0526}$$

and

$$(\delta_a)_A = (\delta_a)_M$$

RESULTS AND DISCUSSION

Static Aileron Effectiveness

Figure 8 presents data obtained on the two-cable mount in terms of rolling moment per degree of aileron deflection plotted against model dynamic pressure. Results are also included in this figure which show a reasonable comparison of data between the two-cable mount and the sting-pylon-spring mount for both the reversal point and rolling moments at conditions below the reversal boundary. Reversal points obtained on the two-cable mount were measured at Mach numbers of 0.675 and 0.75 at model dynamic pressures of 183 lb/ft^2 (8.77 kN/m^2) and 173 lb/ft^2 (8.29 kN/m^2), respectively.

Figure 9 presents the predicted aileron reversal boundary, based on the sting-pylon-spring test results, as a function of Mach number plotted against full-scale dynamic pressure. (Full-scale dynamic pressure is determined from model results by using the relationship $\frac{q_M}{q_A} = 0.26$ obtained from table II.) The reversal boundary is defined by the locus of all zero rolling-moment points obtained. The portion of the curve between $M = 0.84$ and $M = 0.89$ was not determined because excessive buffeting loads developed on the model in this region. The dashed line represents the estimated boundary based on positive effectiveness measurements. The reversal points obtained with the two-cable mount are included in figure 9 and, as indicated previously, show a reasonable comparison between the testing techniques. Flight data presented in figure 9 were obtained from reference 1. Data points at $M = 0.825$ and $M = 0.83$ were obtained

from measured flight data at reversed conditions. The reversal points indicated by ticked symbols were obtained by extrapolating the data to zero control effectiveness. (Representative flight data are presented in a subsequent figure.) Based on the results presented in figure 9, reasonably good correlation exists between the scaled reversal boundary and the measured flight reversal points when an aeroelastic model is used.

<div align="center">Dynamic Results for C_{l_δ} and C_{l_p}</div>

Studies of aileron-control effectiveness were made by using the two-cable mount system at $M = 0.675$ and $M = 0.75$ over a range of model dynamic pressures. At $M = 0.675$ the model dynamic pressures represented scaled flight altitudes of about 4000, 8000, and 11 000 feet (1200, 2400, and 3400 meters). At $M = 0.75$ the scaled flight altitudes were approximately 9000, 12 000, and 16 000 feet (2700, 3700, and 4900 meters). At each discrete dynamic pressure the ailerons were sinusoidally deflected through an amplitude of $\pm 6^o$ over a range of frequencies between 3 and 27 radians/second. This corresponds to a range of reduced frequencies k from about 0.045 to 0.0045 based on $\bar{c}$.

The geometric properties of the two-cable mount system required to evaluate the roll restraint $K_{\varphi\varphi}$ are presented in table III. Measured model dynamic response as a function of aileron frequency, tunnel test conditions, and front and rear cable tensions are presented in table IV. For sinusoidal motion the dynamic amplitude is obtained from the relation $\varphi_0 = \left|\frac{\dot{\varphi}}{\omega}\right|$. The phase angle $\bar{\alpha}$ is obtained by analyzing the signals $\delta_a(t)$ and $\dot{\varphi}(t)$ on an electronic harmonic analyzer. Cable tensions are monitored from the outputs of tension links spliced into the mount.

The solutions of equation (8), based on the measured model response, are presented in figure 10. The results are given in terms of the derivatives C_{l_p} and C_{l_δ} plotted against model dynamic pressure at $M = 0.675$ and $M = 0.75$.

Values of rolling moment per degree of aileron deflection have already been determined at these test conditions during the static tests on the two-cable mount system (see fig. 8), and they thereby provide a comparison between the static and dynamic testing procedures. These comparisons of the aileron-effectiveness derivative C_{l_δ} measured both statically and dynamically are presented in figure 11. At the lower dynamic pressures the results compare quite favorably. At the higher dynamic pressures the static and dynamic results compare less favorably. The reason for this result is probably due to the single-degree-of-freedom assumption that the predominant forcing function generated by the ailerons is the rolling moment. At the higher dynamic pressures the aileron derivative is significantly reduced, and, therefore, the ailerons produce less rolling motion compared with motion in the other degrees of freedom.

Figure 12 presents typical measured flight data, obtained from reference 1, in terms of roll rate plotted against flight dynamic pressures at nominal altitudes of 14 000,

16 000, 20 000, and 30 000 feet (4300, 4900, 6100, and 9100 meters). The flight data are based on aileron deflections of approximately 20°. Dynamic pressures corresponding to $M = 0.675$ and $M = 0.75$ at various altitudes are indicated in the figure.

Once the nondimensional aerodynamic derivatives C_{l_p} and C_{l_δ} are obtained from model tests (fig. 11), these values can be substituted into equation (9) to predict the free-flight roll rate $\dot{\varphi}_A$ at the properly scaled dynamic pressure and Mach number. A comparison of predicted and measured flight roll rates is presented in figure 13 in terms of full-scale roll rate (20° aileron deflection) plotted against airplane dynamic pressures at $M = 0.675$ and $M = 0.75$. The curves are extrapolated to zero effectiveness by using the measured model reversal points. The data presented in figure 13 show a reasonable comparison between predicted and measured flight-control effectiveness even though a single-degree-of-freedom approximation was used.

CONCLUSIONS

Wind-tunnel studies of an aeroelastically and dynamically scaled model of a multijet cargo airplane have been conducted to measure the full-scale aileron reversal boundary and aileron-control effectiveness at Mach numbers up to 0.93. Model results obtained in the wind tunnel have been compared directly with those obtained in flight.

The following conclusions can be drawn from this investigation:

1. Static and dynamic results obtained with the model have established a successful method for experimentally determining the flight aileron effectiveness and damping in roll.

2. Flight roll rates at dynamic pressures somewhat below the reversal boundary have been predicted based on wind-tunnel measurements of a flexible model tested on the two-cable mount system.

Langley Research Center,
    National Aeronautics and Space Administration,
        Langley Station, Hampton, Va., August 4, 1969.

REFERENCES

1. Anon.: C-141A Aileron Control System Effectiveness. Rep. No. ER 6305, Lockheed-Georgia Co., June 28, 1963.

2. Grosser, William F.: A Transonic Speed Wind Tunnel Investigation of the Rolling Effectiveness of a Large Swept Wing Transport Aircraft With Conventional Type Ailerons and Various Spoiler Configurations. AIAA Paper No. 65-789, Nov. 1965.

3. Guyett, P. R.: The Use of Flexible Models in Aerospace Engineering. Tech. Rep. No. 66335, Brit. R.A.E., Nov. 1966.

4. Reed, Wilmer H., III; and Abbott, Frank T., Jr.: A New "Free-Flight" Mount System for High-Speed Wind-Tunnel Flutter Models. Proceedings of Symposium on Aero-elastic & Dynamic Modeling Technology, RTD-TDR-63-4197, Pt. I, U.S. Air Force, Mar. 1964, pp. 169-206.

5. Abel, Irving: A New Wind-Tunnel Technique for the Measurement of Various Aircraft Stability Derivatives. M.S. Thesis, Univ. of Virginia, 1968.

6. Mechtly, E. A.: The International System of Units — Physical Constants and Conversion Factors. NASA SP-7012, 1964.

7. Etkin, Bernard: Dynamics of Flight — Stability and Control. John Wiley & Sons, Inc., c.1959.

TABLE I.- GEOMETRIC AND MASS PROPERTIES OF MODEL

(a) Geometric properties

Wing:
Area, sq ft (m²) 8.94 (0.831)
Span, ft (m) 8.46 (2.58)
Aspect ratio 8.01
Taper ratio 0.373
Sweep at 0.25 chord, deg —
  Inboard 23.7
  Outboard 25.0
Mean aerodynamic chord, ft (m) 1.17 (0.357)
Aileron area, sq ft (m²) 0.468 (0.0435)

Horizontal tail:
Area, sq ft (m²) 1.51 (0.140)
Span, ft (m) 2.82 (0.86)
Aspect ratio 5.26
Taper ratio 0.37
Sweep at 0.25 chord, deg 25.0
Mean aerodynamic chord, ft (m) 0.58 (0.177)

Vertical tail:
Area, sq ft (m²) 1.15 (0.107)
Aspect ratio 1.24
Taper ratio 0.61
Sweep at 0.25 chord, deg 35.0
Mean aerodynamic chord, ft (m) 0.98 (0.299)

(b) Mass properties

Weight, lb (N) 47.9 (213.0)

Center-of-gravity location, percent $\bar{c}$ 25.0

Moments of inertia about center of gravity, slug-ft² (kg-m²):
Pitch, I_Y 2.79 (3.78)
Roll, I_X 2.16 (2.93)
Yaw, I_Z 4.28 (5.80)

TABLE II.- MODEL SCALE FACTORS

Parameter	Scale factor	
	Relationship	Value
Geometric	b_M/b_A	0.0526
Mach number	M_M/M_A	1.0
Reduced frequency	$(U/b\omega)_M/(U/b\omega)_A$	1.0
Mass ratio	$(Mass/\rho b^3)_M/(Mass/\rho b^3)_A$	1.0
Froude number	$(gb/U^2)_M/(gb/U^2)_A$	0.304
Density	ρ_M/ρ_A	1.5
Velocity	U_M/U_A	0.416
Frequency	ω_M/ω_A	7.92
Weight (W)	W_M/W_A	0.000219
Dynamic pressure	q_M/q_A	0.26
Moment of inertia (I) . . .	I_M/I_A	0.606×10^{-6}
Stiffness	$(EI)_M/(EI)_A$ or $(GJ)_M/(GJ)_A$	0.2×10^{-5}

TABLE III.- GEOMETRIC PROPERTIES OF THE TWO-CABLE MOUNT

SYSTEM USED IN THIS INVESTIGATION

h, ft (m) 0.37 (0.113)

d, ft (m) 0.39 (0.119)

L_f, ft (m) 23.0 (7.01)

L_r, ft (m) 23.0 (7.01)

β_f, deg 20.0

β_r, deg 20.0

a, ft (m) . . . . [a]1.2 (0.366)

c, ft (m) . . . . [a]1.0 (0.305)

[a]Required values of front and rear pulley spacing for single-degree-of-freedom assumption (ref. 5).

TABLE IV.- MEASURED DYNAMIC RESPONSE OF MODEL

| ω, rad/sec	ϕ_o, deg	$\overline{\alpha}$, deg	M	q lb/ft^2	q kN/m^2	U ft/sec	U m/sec	T_f lb	T_f N	T_r lb	T_r N
26.4	0.011	−159	0.675	115	5.51	350	107	130	578	100	445
22.8	.013	−150	↓	↓	↓	↓	↓	↓	↓	↓	↓
21.4	.016	−147									
18.3	.019	−136									
16.6	.021	−117									
13.8	.022	−112									
10.8	.029	−101									
8.9	.038	−99									
6.7	.051	−86									
4.3	.072	−66	↓	↓	↓	↓	↓	↓	↓	↓	↓
25.5	.010	−158	.675	130	6.23	350	107	138	614	100	445
22.1	.013	−147	↓	↓	↓	↓	↓	↓	↓	↓	↓
20.9	.014	−143									
17.7	.018	−116									
15.7	.018	−107									
13.8	.021	−111									
11.6	.024	−109									
9.3	.031	−99									
5.1	.055	−72									
3.9	.064	−62									
2.9	.076	−53	↓	↓	↓	↓	↓	↓	↓	↓	↓
26.6	.0088	−159	.675	150	7.19	350	107	144	641	100	445
24.4	.0103	−151	↓	↓	↓	↓	↓	↓	↓	↓	↓
22.9	.012	−147									
21.6	.013	−138									
19.4	.015	−116									
16.7	.014	−107									
14.8	.014	−114									
11.6	.020	−103									
8.8	.025	−97									
7.4	.031	−92									
6.6	.036	−85									
4.1	.052	−69	↓	↓	↓	↓	↓	↓	↓	↓	↓
26.9	.009	−162	.75	117	5.61	397	121	128	569	100	445
24.8	.011	−157	↓	↓	↓	↓	↓	↓	↓	↓	↓
22.9	.013	−151									
21.5	.014	−150									
19.4	.016	−139									
16.7	.018	−124									
14.7	.020	−124									
12.0	.025	−117									
9.3	.033	−98									
7.0	.042	−92									
3.5	.076	−55	↓	↓	↓	↓	↓	↓	↓	↓	↓
26.6	.008	−160	.75	155	6.47	397	121	138	614	100	445
24.2	.009	−154	↓	↓	↓	↓	↓	↓	↓	↓	↓
22.4	.011	−151									
21.4	.012	−147									
19.4	.014	−138									
16.7	.014	−119									
14.3	.015	−120									
11.5	.023	−104									
8.6	.029	−100									
7.3	.032	−89									
5.7	.046	−82									
3.4	.064	−56	↓	↓	↓	↓	↓	↓	↓	↓	↓
23.9	.008	−153	.75	152	7.28	397	121	145	645	100	445
22.9	.009	−151	↓	↓	↓	↓	↓	↓	↓	↓	↓
21.7	.009	−147									
20.0	.010	−132									
17.7	.011	−121									
15.7	.012	−115									
13.8	.012	−118									
11.2	.016	−104									
8.7	.021	−93									
7.0	.026	−85									
6.2	.030	−83									
5.0	.040	−69									
3.9	.043	−63	↓	↓	↓	↓	↓	↓	↓	↓	↓
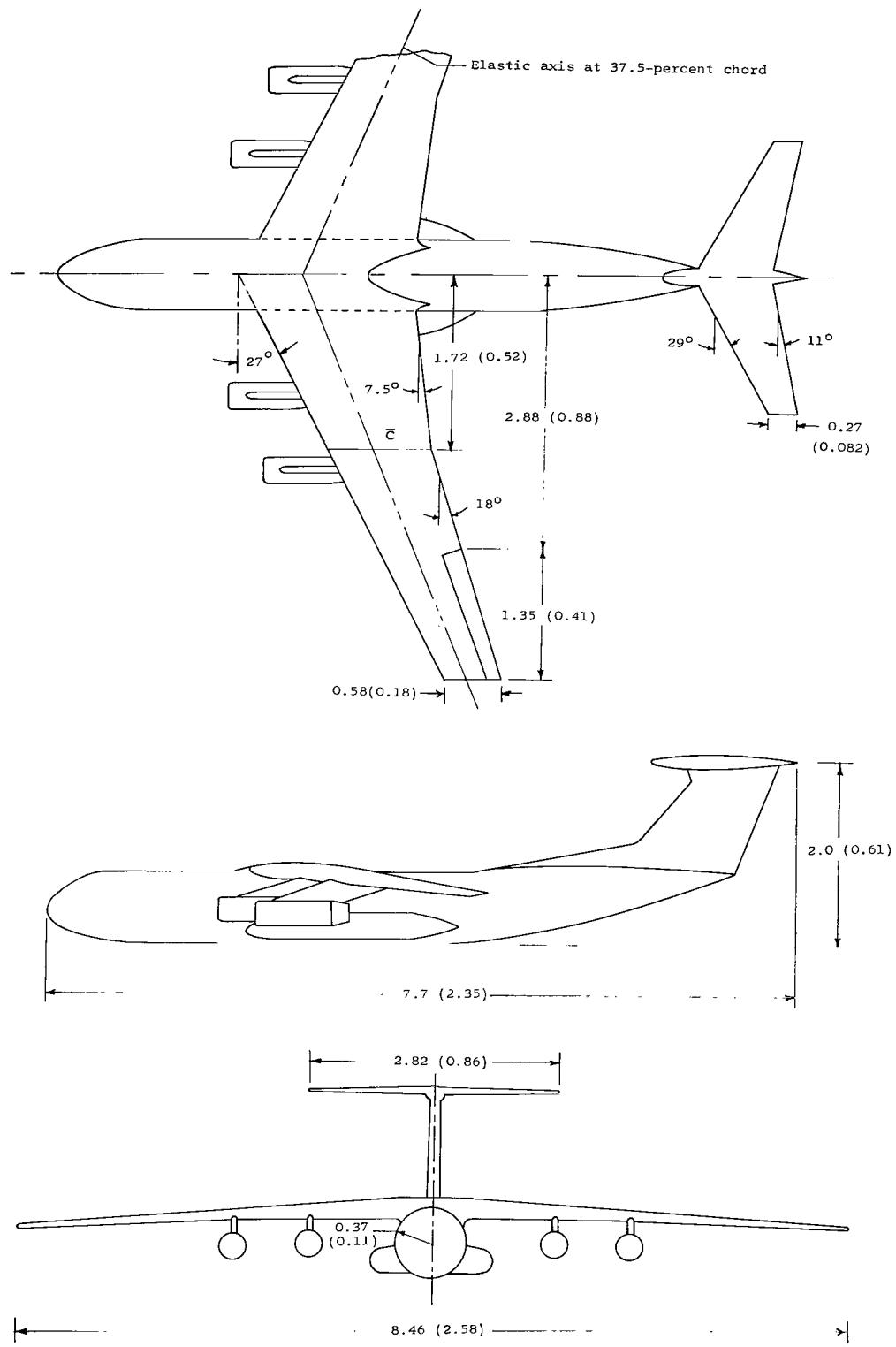
Figure 1.- Three views of model. (Linear dimensions are given in feet and parenthetically in meters.)

18
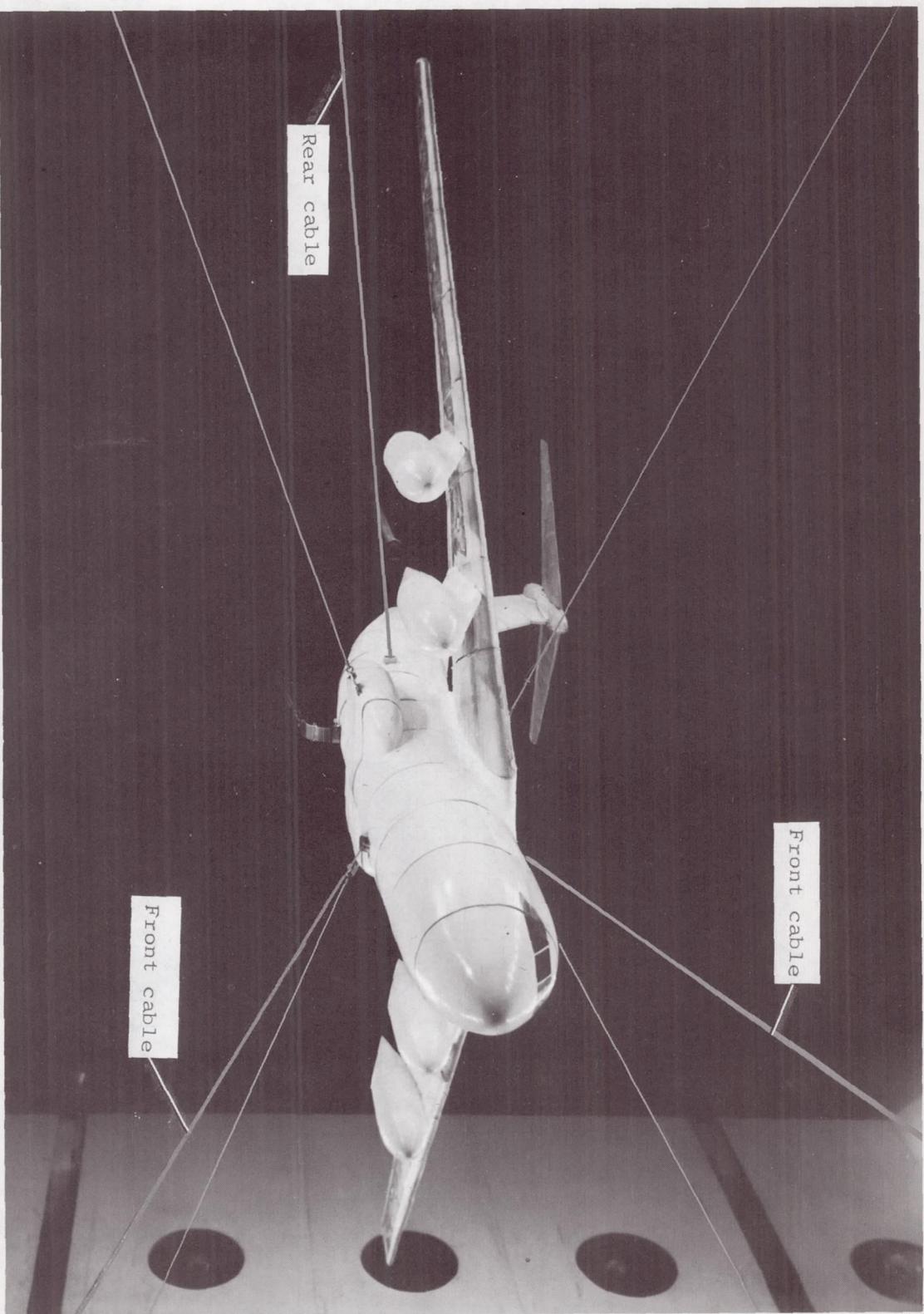
Figure 2.- Photograph of model on two-cable mount system.

Rear cable

Front cable

Front cable

L-66-5000.1
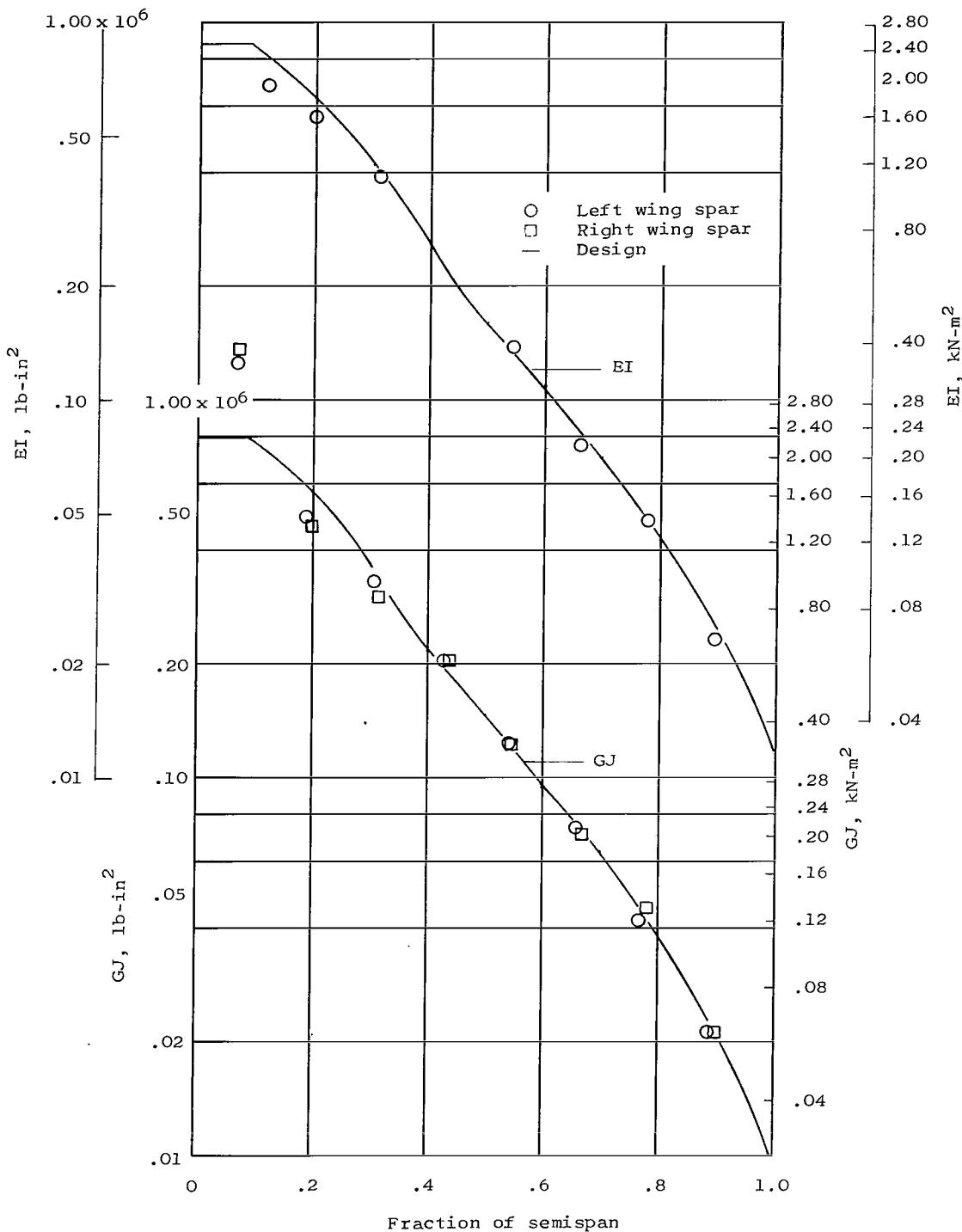
Figure 3.- Measured distribution of bending and torsional stiffnesses of model wing spar.
(EI and GJ measured perpendicular to wing elastic axis.)

Silked balsa fairing

Section attachment points

Magnesium spar

Balsa
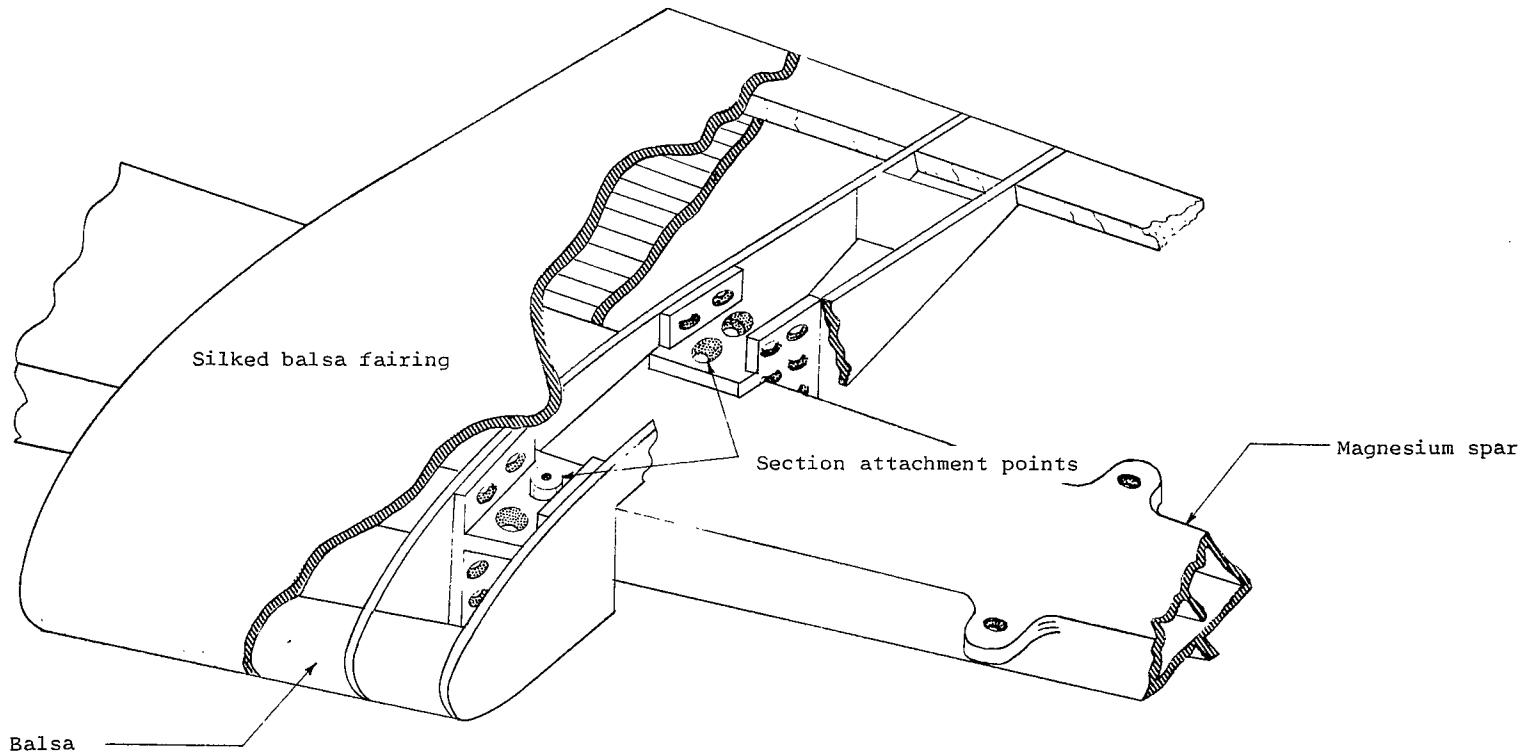
Figure 4.- Cutaway view of typical spar section.
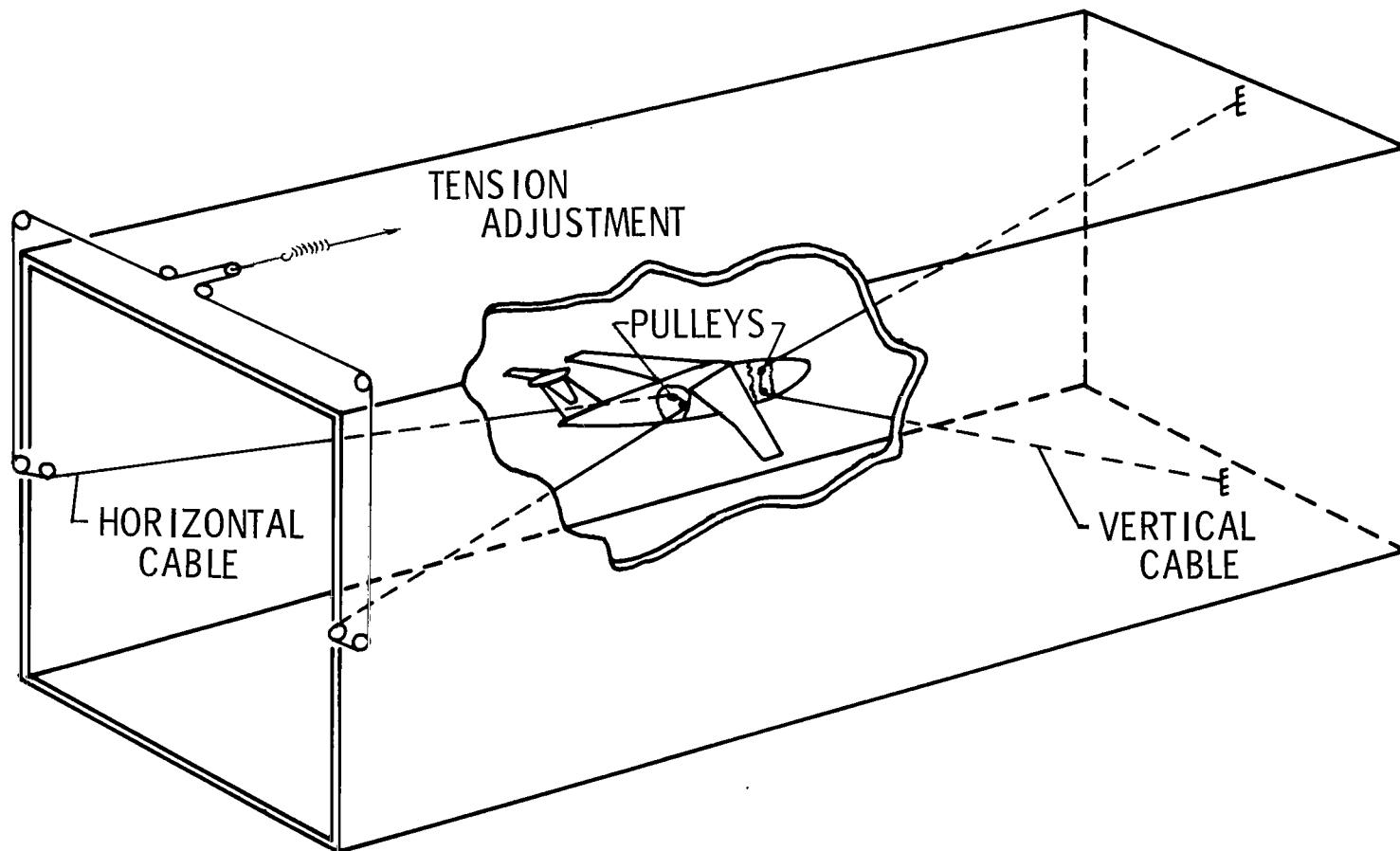
(a) Model on mount.

Figure 5.- Two-cable mount system.
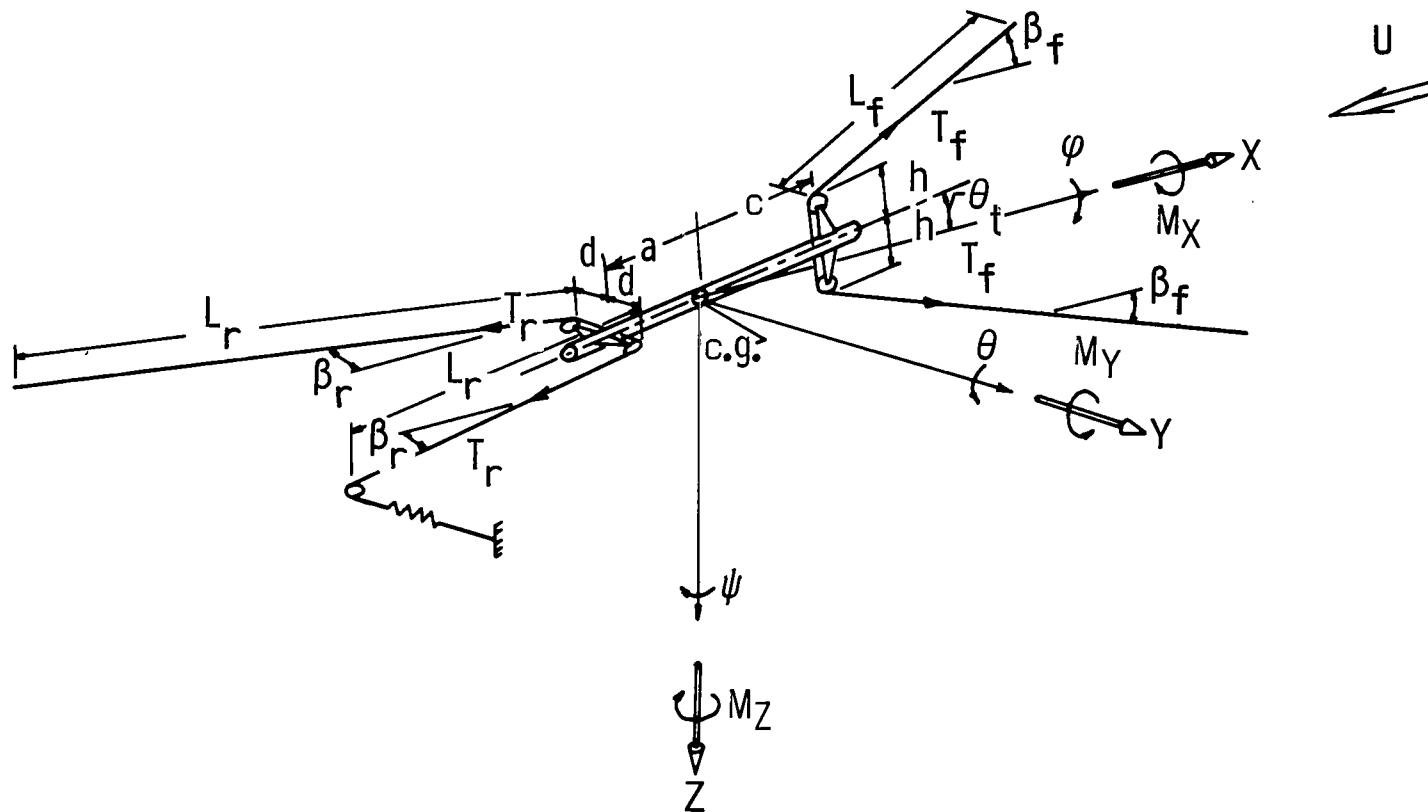
(b) Mount geometry.

Figure 5.- Concluded.
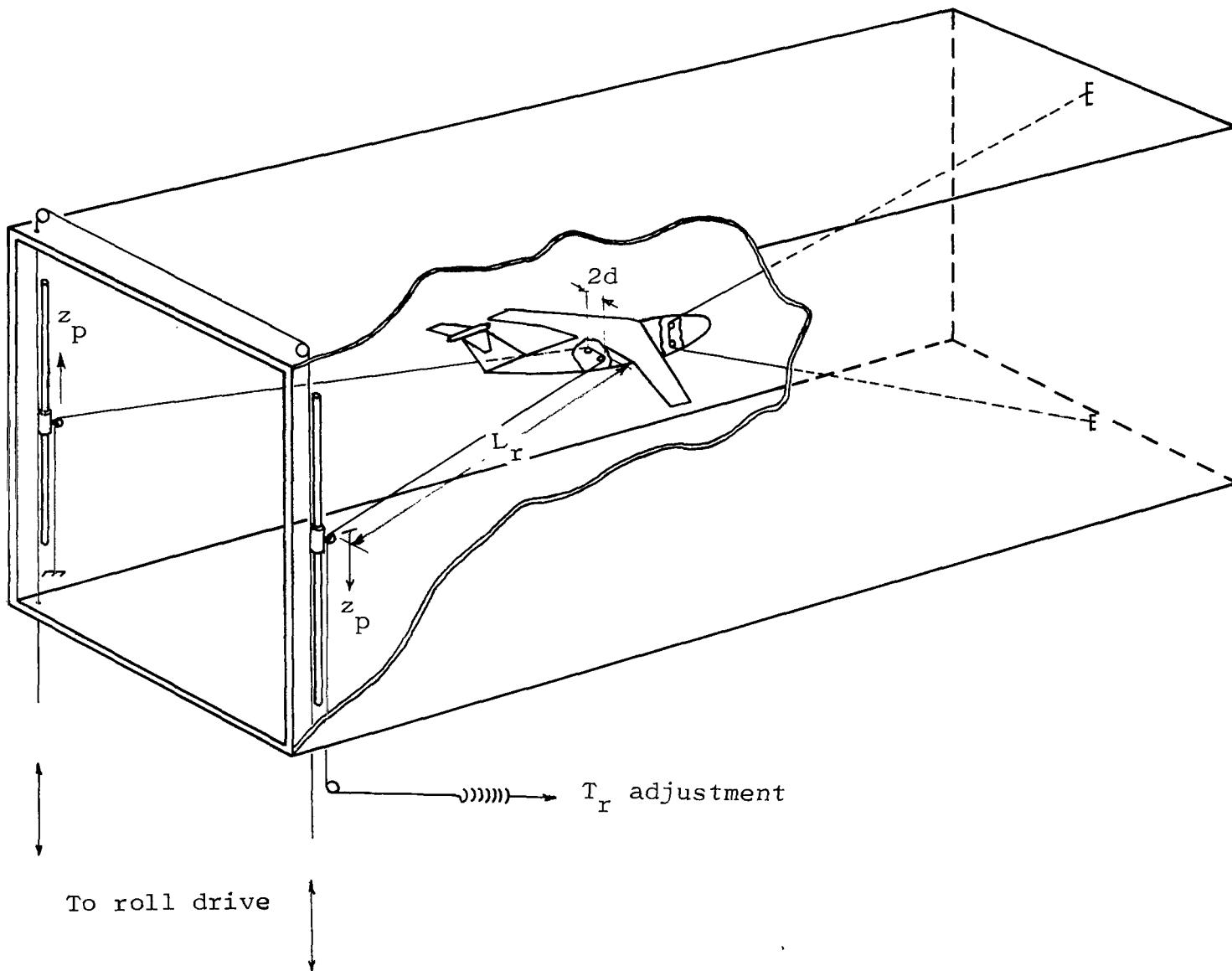
Figure 6.- Two-cable mount system with roll device.
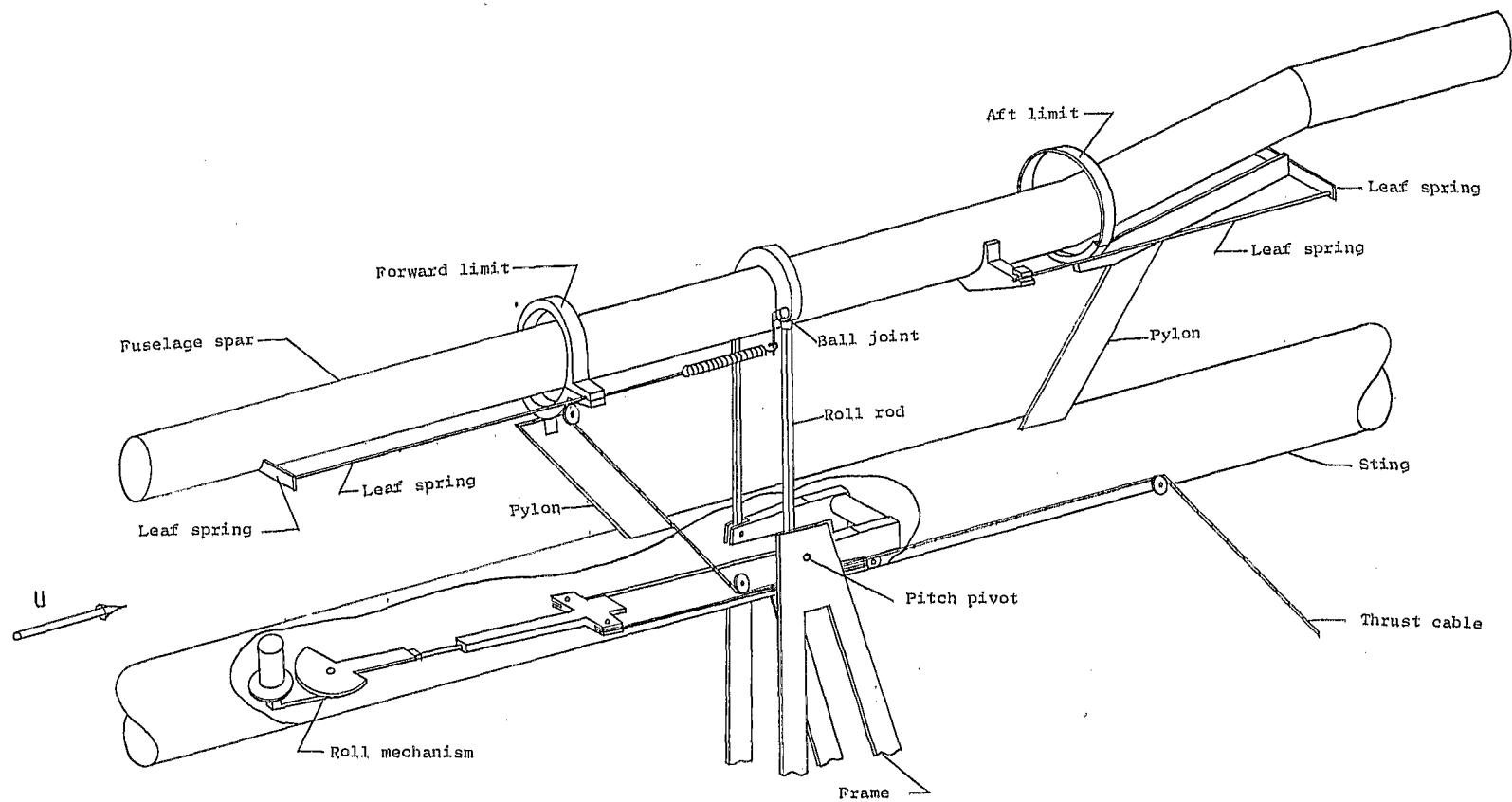
Figure 7.- Sting-pylon-spring mount system.
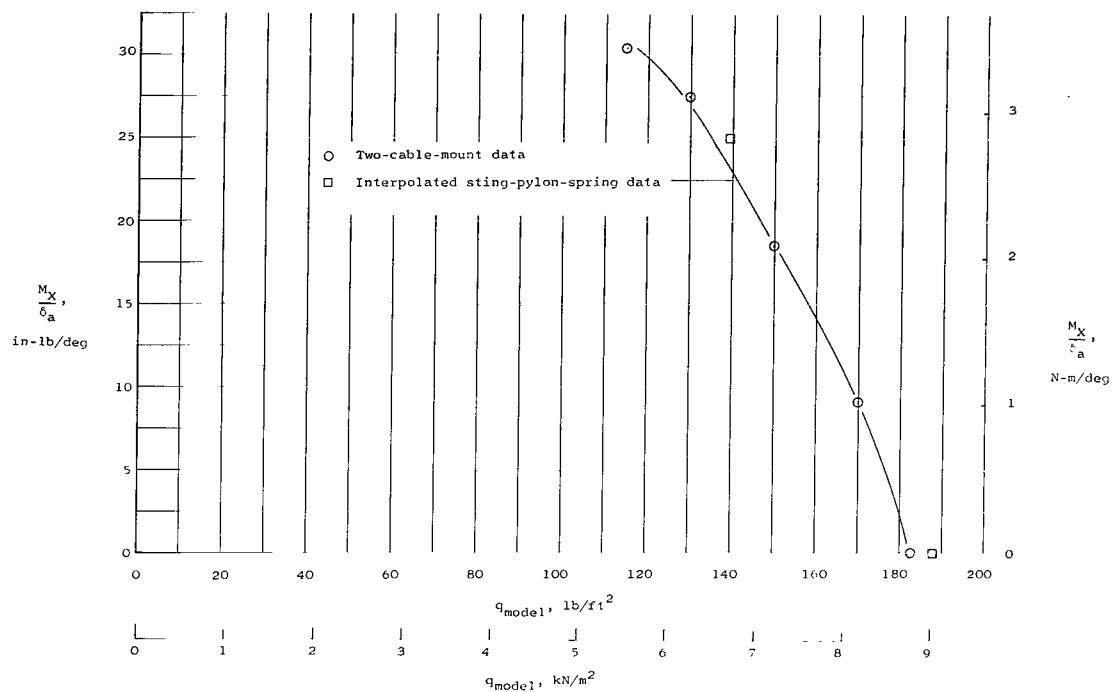
(a) M = 0.675.
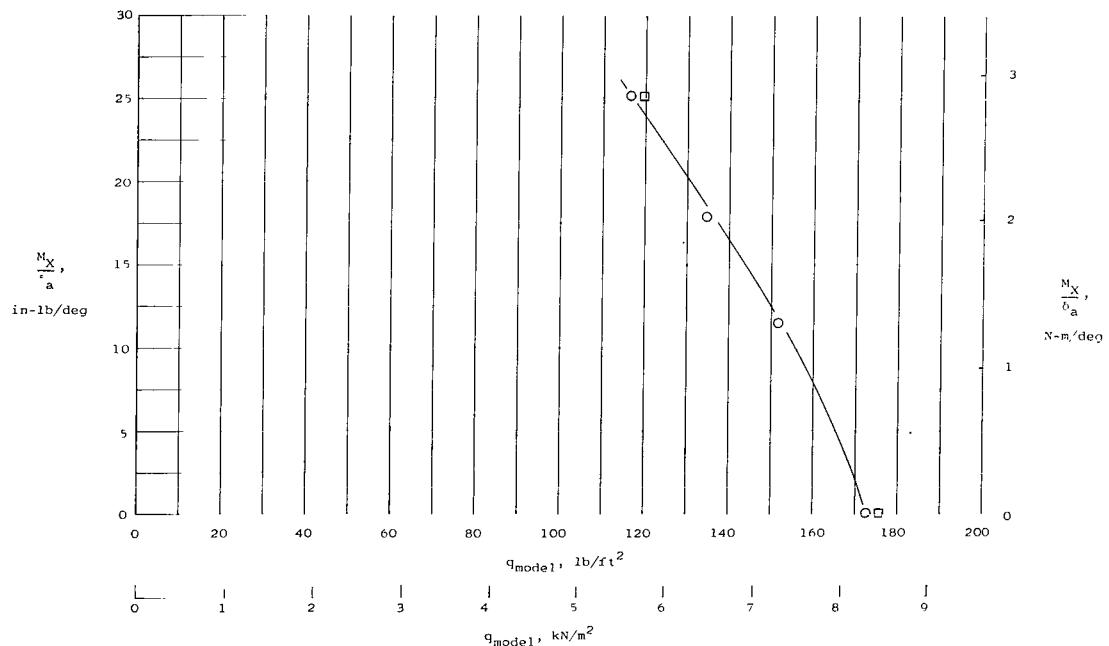
(b) M = 0.75.

Figure 8.- Average measured rolling moments.
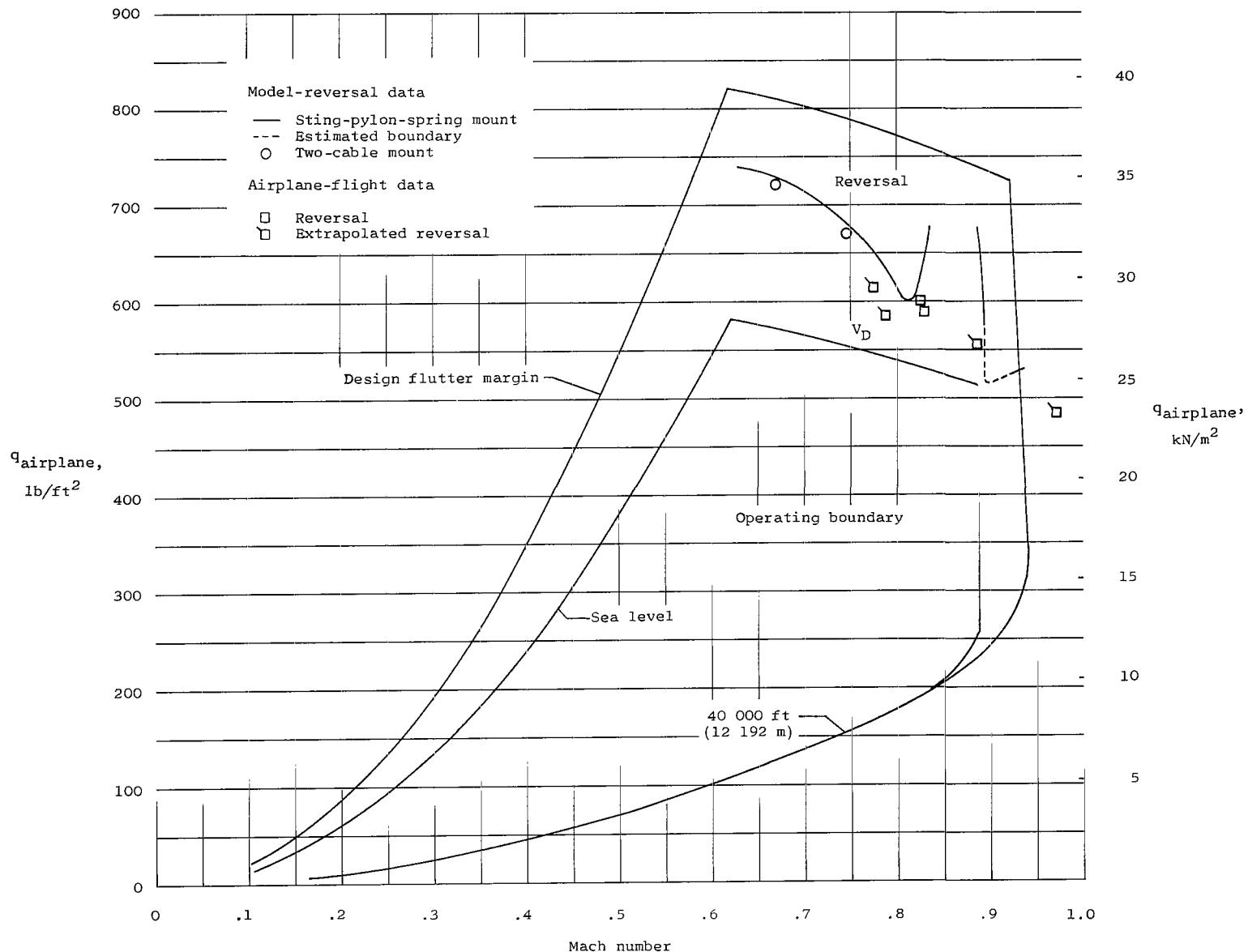
Figure 9.- Comparison of model aileron reversal boundary with full-scale flight data. (Flight data obtained from reference 1.)
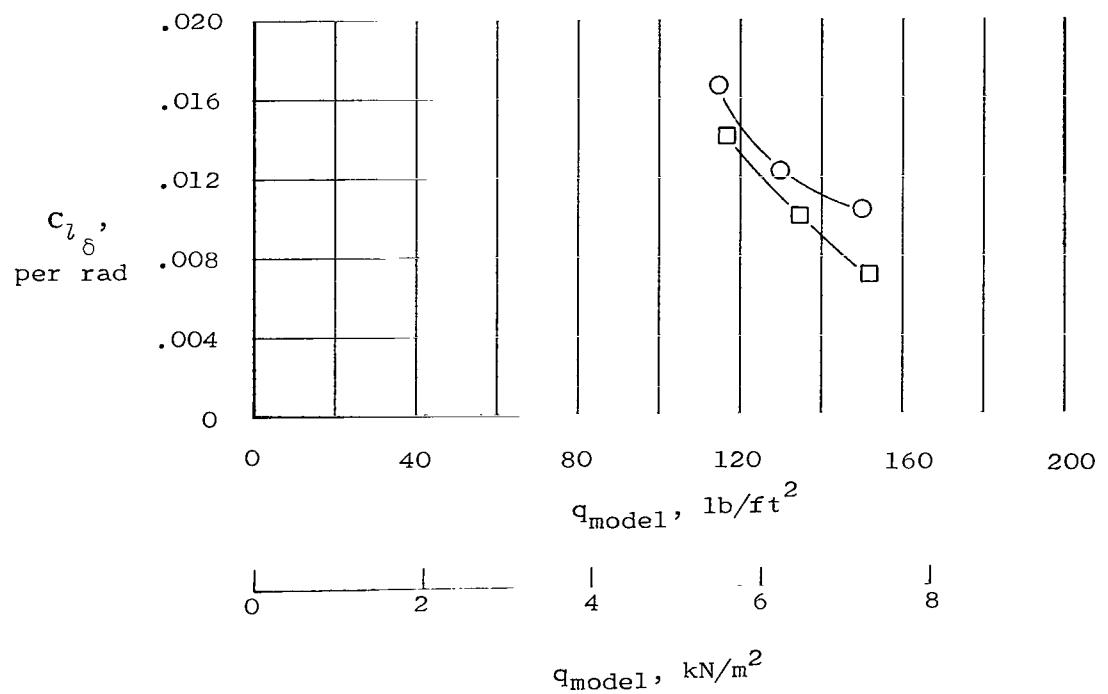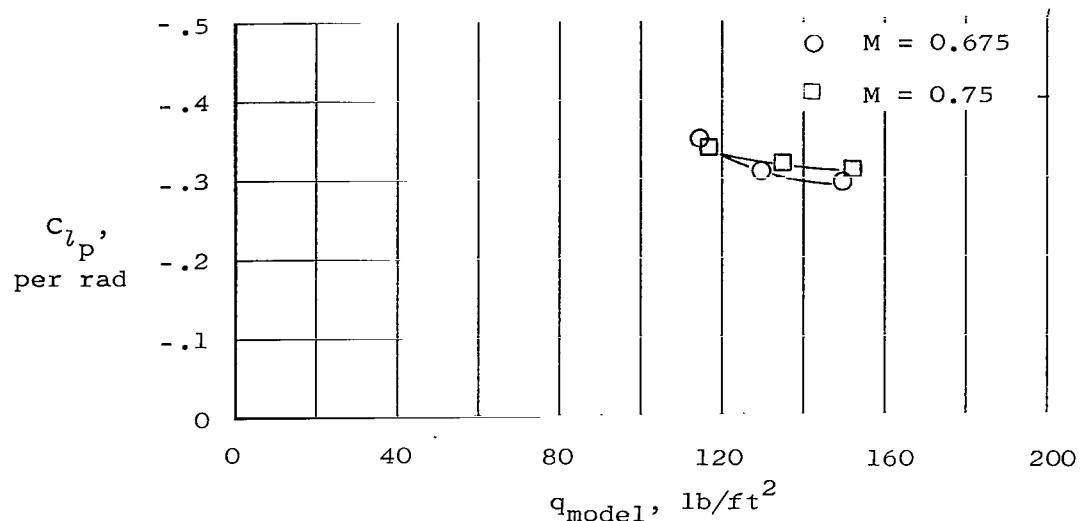
Figure 10.- Aerodynamic derivatives measured on two-cable mount system.
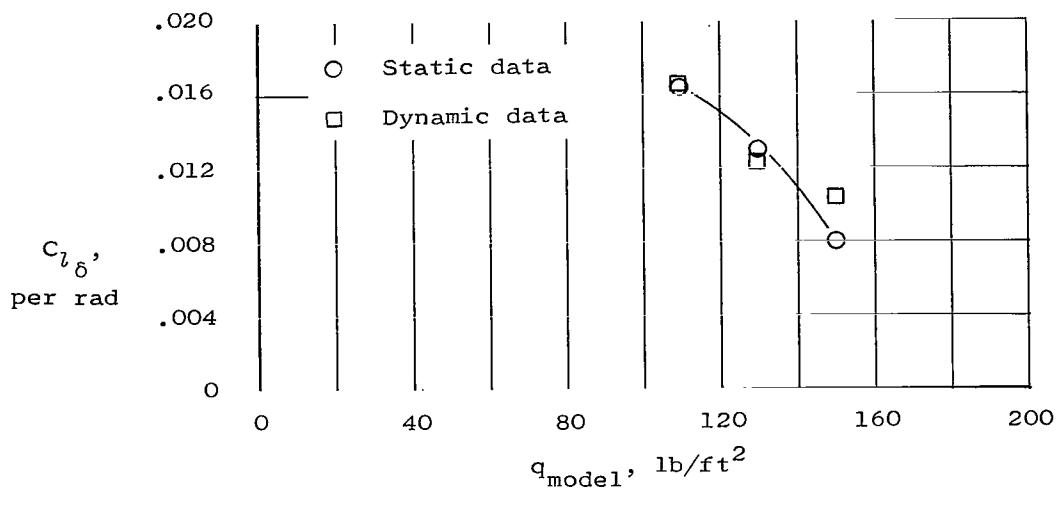
(a) M = 0.675.
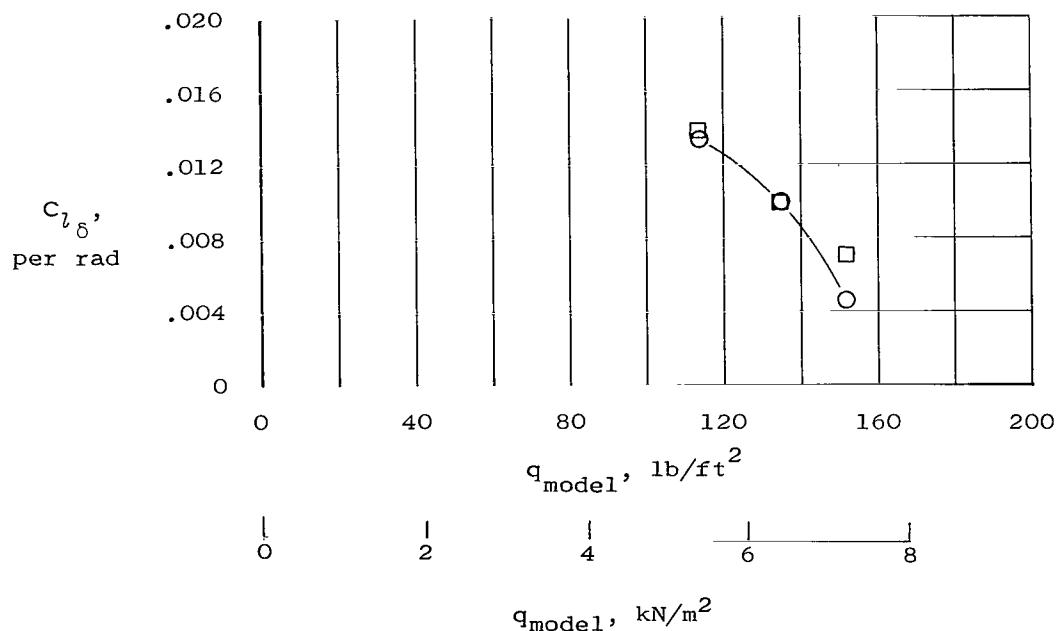
(b) M = 0.75.

Figure 11.- Comparison of static and dynamic experimental results.
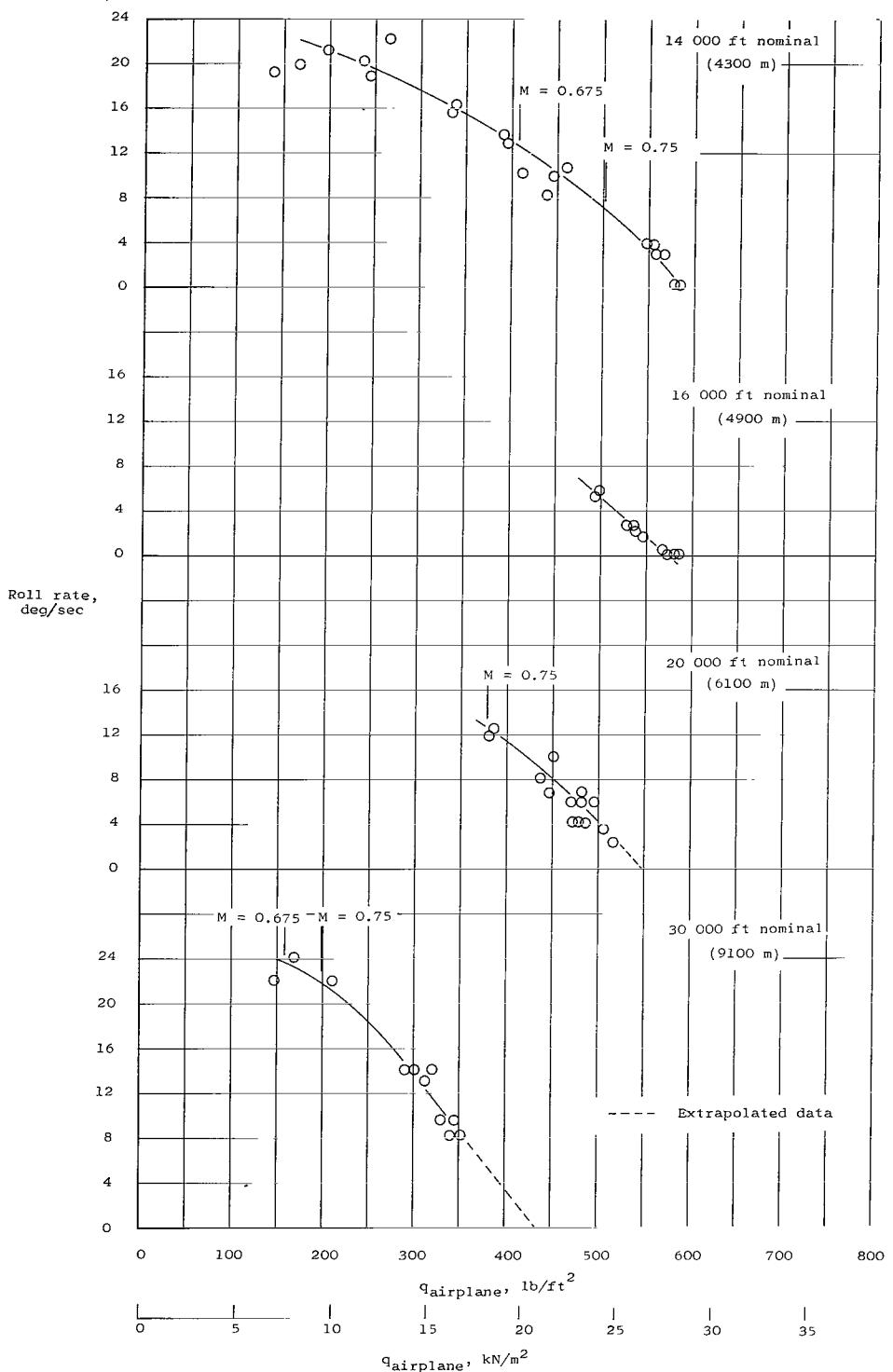
Figure 12.- Roll rate measured from flight with approximately 20⁰ aileron deflection. (Data obtained from reference 1.)
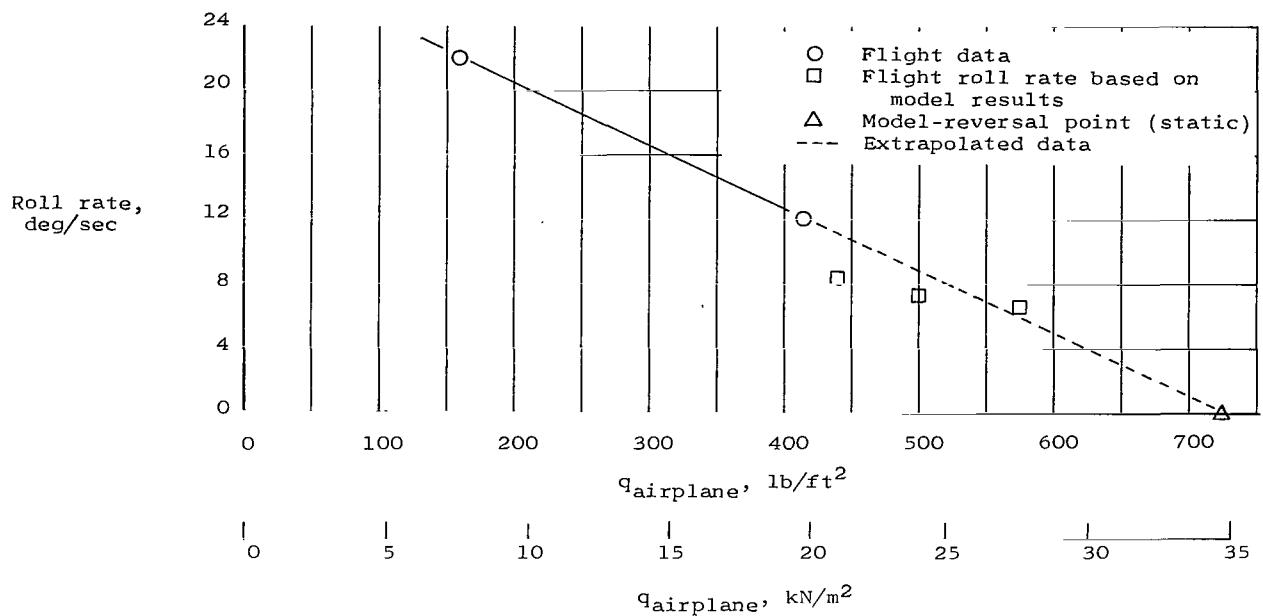
(a) M = 0.675.
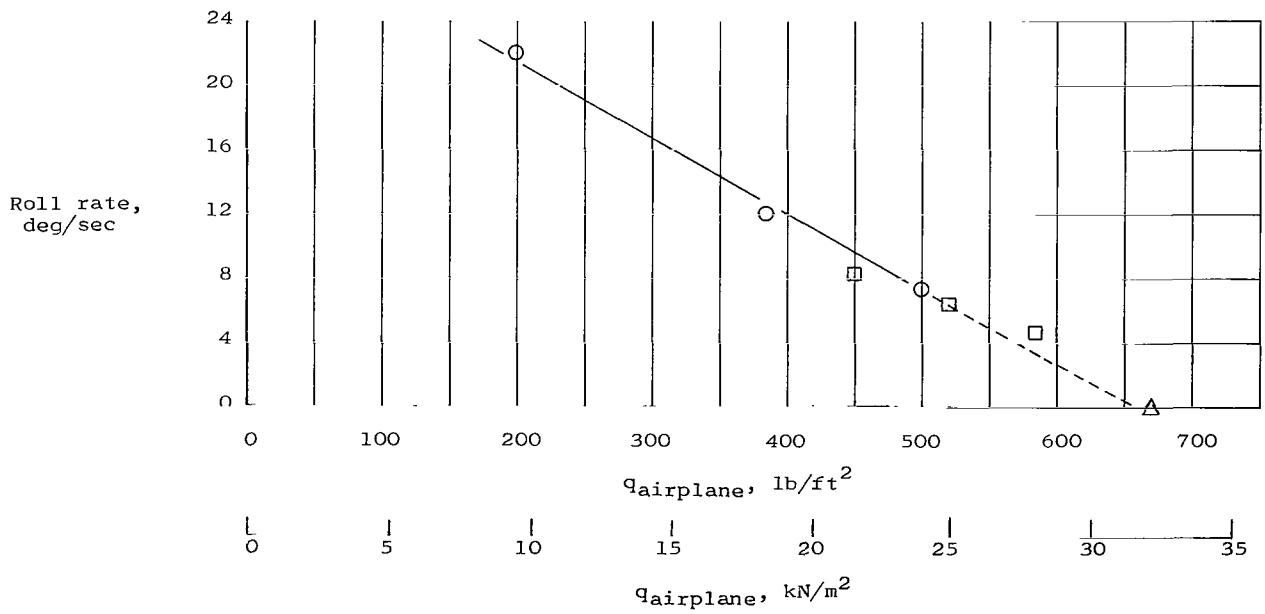
(b) M = 0.75.

Figure 13.- Comparison of predicted and measured flight roll rates. $(\delta_a)_A = 20^0$.
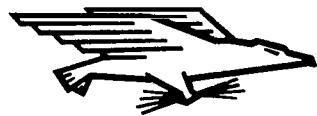
"The aeronautical and space activities of the United States shall be
conducted so as to contribute . . . to the expansion of human knowl-
edge of phenomena in the atmosphere and space. The Administration
shall provide for the widest practicable and appropriate dissemination
of information concerning its activities and the results thereof."

— NATIONAL AERONAUTICS AND SPACE ACT OF 1958

NASA SCIENTIFIC AND TECHNICAL PUBLICATIONS

TECHNICAL REPORTS: Scientific and
technical information considered important,
complete, and a lasting contribution to existing
knowledge.

TECHNICAL NOTES: Information less broad
in scope but nevertheless of importance as a
contribution to existing knowledge.

TECHNICAL MEMORANDUMS:
Information receiving limited distribution
because of preliminary data, security classifica-
tion, or other reasons.

CONTRACTOR REPORTS: Scientific and
technical information generated under a NASA
contract or grant and considered an important
contribution to existing knowledge.

TECHNICAL TRANSLATIONS: Information
published in a foreign language considered
to merit NASA distribution in English.

SPECIAL PUBLICATIONS: Information
derived from or of value to NASA activities.
Publications include conference proceedings,
monographs, data compilations, handbooks,
sourcebooks, and special bibliographies.

TECHNOLOGY UTILIZATION
PUBLICATIONS: Information on technology
used by NASA that may be of particular
interest in commercial and other non-aerospace
applications. Publications include Tech Briefs,
Technology Utilization Reports and Notes,
and Technology Surveys.

Details on the availability of these publications may be obtained from:

SCIENTIFIC AND TECHNICAL INFORMATION DIVISION

NATIONAL AERONAUTICS AND SPACE ADMINISTRATION
Washington, D.C. 20546